INVESTIGATIONS ON NOISE SOURCES ON A CONTRA-ROTATING AXIAL FAN WITH DIFFERENT MODIFICATIONS

Ralph KRAUSE[1], Christian FRIEBE[1], Michael KERSCHER[2], Christof PUHLE[3]

[1] *INSTITUT FÜR LUFT- UND KÄLTETECHNIK gGmbH, Bertolt-Brecht-Allee 20, 01309 Dresden, Germany*

[2] *GFAI TECH GmbH, Volmerstraße 3, 12489 Berlin, Germany*

[3] *GFAI Gesellschaft zur Förderung angewandter Informatik e.V., Volmerstraße 3, 12489 Berlin, Germany*

SUMMARY

An Acoustic Camera was applied to examine modifications of fan blade designs regarding their noise emissions. A so-called rotational beamforming algorithm allows for the detection of sound sources on the rotating blades by using a virtual rotation of the microphones. Depending upon the frequency different sources could be localized. Both the leading and trailing edge were modified, however only results of the modification on trailing edge are represented in this paper. The trailing edge was modified using serrations, which shall lead to vortices at higher frequencies. This paper shows the performed modifications and tests with the Acoustic Camera. It also presents first results and gives an outlook on future work and usage.

INTRODUCTION

Axial blowing fans are commonly known in many fields of applications. By using axial fans swirls occur at the trailing edge of the blades due to the working principle. These swirls are unwanted in most cases and may have unfavourable influence on subsequent devices, e.g. higher pressure drop or lower heat transfer coefficient. As the static pressure rise is an evaluation criterion for the fan efficiency there are different possibilities for converting the dynamic pressure of the swirl into a static pressure rise. The most common application for rising the efficiency is the installation of outlet guide vanes.

The installation of contra-rotating axial fans (CRF) is another well-known opportunity to increase the efficiency of a fan. Beside the high power density and the high efficiency it should be noted that these fans are known for problematic noise behaviour. This is induced by the interaction of both wheels with different directions of rotation.

The aim of the project is to investigate the influence of different suggestions of literature on how to reduce the noise emission of fans based on modifications of the blade design. Therefore a CRF with different blade couples is used to measure the noise emission. To localize the noise sources a so-called Acoustic Camera with a special beamforming algorithm was used [13].

WORKING PRINCIPLE CONTRA-ROTATING FAN

Due to the Euler equation the specific work is defined by

$$Y = u'' c_u'' - u' c_u'. \tag{1}$$

For an axial fan stage obviously $u'' = u' = u$, which transforms eq. (1) to

$$Y = u(c_u'' - c_u'), \tag{2}$$

with u being the amount of the circumferential speed, c_u the component of the fluid velocity vector $\boldsymbol{c}$ with the same direction of $\boldsymbol{u}$ and $'$ as inlet and $''$ as outlet symbols.

According to eq. (2) a pressure rise in an axial impeller stage causes a change in the outflow $c_{A,u}'' \neq 0$ compared to the inlet conditions $c_{A,u}' = 0$. The second impeller, with an opposite direction of rotation, shall be designed without outlet swirl as there is already a swirl at the inlet $c_{B,u}' < 0$. Figure 1 represents the velocity components for a contra rotating axial fan stage without outlet swirl, defined by $c_u'' = 0$.

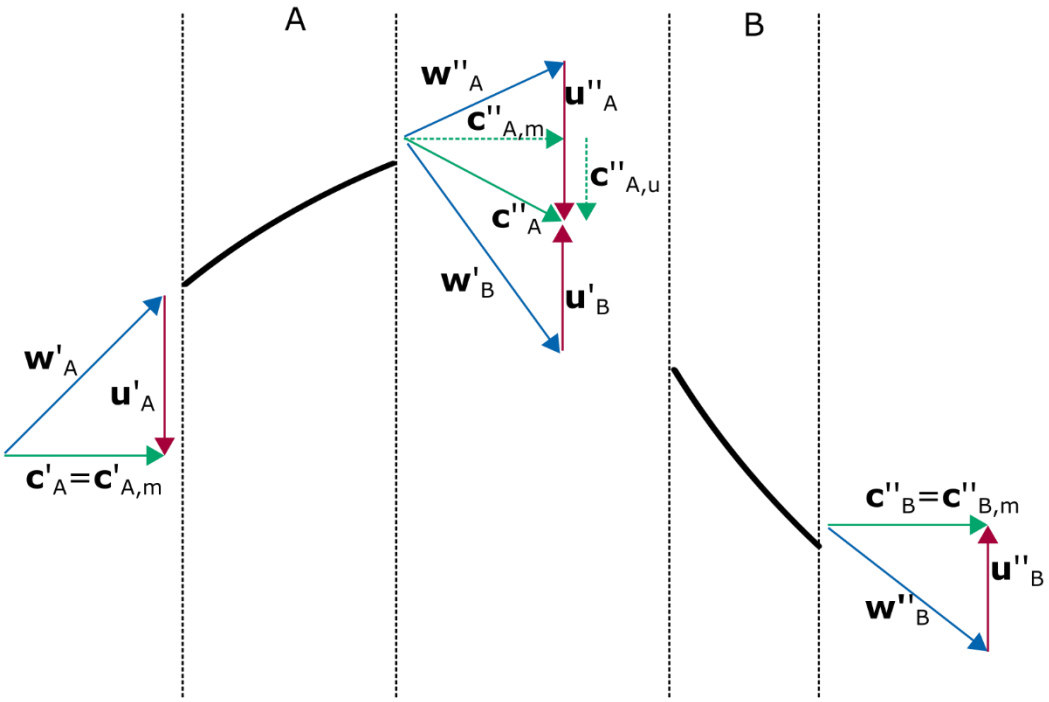

Figure 1: schematic representation of the velocity components

The fan configuration used in this paper corresponds to the schematic drawing as presented in Figure 2. Each impeller (A, B) is driven with a separate motor. Stationary components and rotating

components are differently coloured. Stationary components are presented in black and rotating components are coloured in blue and red, according to their direction of rotation.

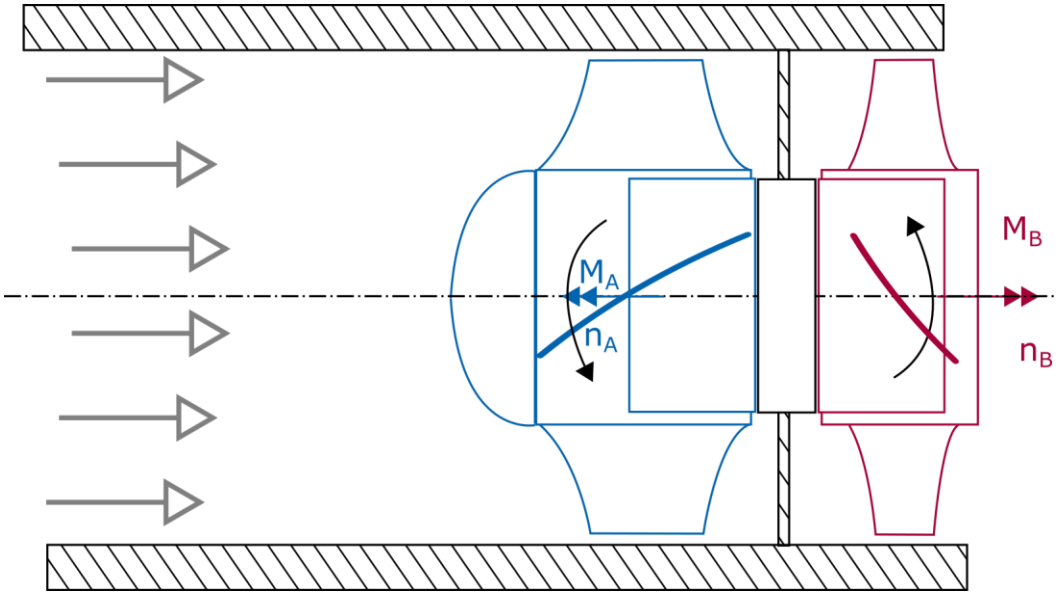

Figure 2: schematic representation of the CRF-construction with one drive for each impeller

ROTATIONAL BEAMFORMING

Functional Beamforming

Let M be the number of microphones of a phased array and $C \in C^M$ the corresponding matrix of auto- and cross-spectra resulting from an averaged short-time FFT of a measurement. Then, in the frequency domain formulation of delay-and-sum beamforming (FDBF), the map value at a point $x_i \in R^3$ is given by

$$B(x_i) = h^H(x_i) C h(x_i) \tag{3}$$

where the superscript H denotes the conjugate transpose and $h^H(x_i) \in C^M$ is the steering vector of type I of x_i (see [3]). The auto-spectra in the diagonal of C do not contain any information about phase differences between the signals. Consequently, they are often removed in order to reduce the error introduced by uncorrelated background noise.

Caused by fundamental properties of the beamforming approach and the chosen array geometry, the map B is a convolution of the actual source distribution with a point spread function leading to high side-lobe levels and limiting the dynamic range of the acoustic map.

To overcome this problem deconvolution methods have been proposed to decompose C into parts representing individual sources (see [1], [2] and [4]). Among them, functional beamforming (FB) is particularly useful to increase the dynamic range. In addition, it allows for a combination with the decomposition approach of orthogonal beamforming (OB).

Since C is self-adjoint by definition, there exist $\lambda_1, \dots, \lambda_M \in R$ and an orthogonal basis $u_1, \dots, u_M \in C^M$ such that

$$C = \sum_{m=1}^{M} \lambda_m u_m u_m^H \tag{4}$$

Each summand $\lambda_m u_m u_m^H \in C^{M\times M}$ is called component of C. Suppose that C is positive definite. Then $\lambda_1, \dots, \lambda_M > 0$ and

$$C^{\frac{1}{v}} \coloneqq \sum_{m=1}^{M} \lambda_m^{\frac{1}{v}} u_m u_m^H \tag{5}$$

is well defined for $v \in N, v \geq 1$. Now the value of the functional beamforming map of order v at x_i can be defined as

$$B_\mu^v(x_i) \coloneqq \left(h^H(x_i) C^{\frac{1}{v}} h(x_i) \right)^v. \tag{6}$$

In many cases throughout this article we assume $\lambda_1 \geq \cdots \geq \lambda_M$ and consider only the first $\mu \in N$, $\mu \geq 1$ components, i.e. we use the reduced functional beamforming map B_μ^v of order v:

$$B_\mu^v(x_i) \coloneqq \left(h^H(x_i) C^{\frac{1}{v}} h(x_i) \right)^v, C^{\frac{1}{v}} \coloneqq \sum_{m=1}^{M} \lambda_m^{\frac{1}{v}} u_m u_m^H \tag{7}$$

Virtual Array Rotation

The methods of the previous section are based on the assumption that the phased array and the measured object are fixed spatially to each other. Since this is obviously not the case when measuring a rotating fan, we determine the signals of a virtual microphone array that is fixed in the coordinate system of the fan. For each point in time t let $p_1^v(t), \dots p_M^v(t) \in R^3$ denote the microphone positions of the virtual array in the coordinate system of the array measurement at $p_1(t), \dots p_M(t) \in R^3$. The signal value $s_i^v(t_0)$ of the *i*-th virtual microphone at t_0 is determined as follows. We compute the two nearest neighbours pk, pl of p_i^v among the measurement positions and set

$$s_1^v(t_0) = \frac{\|p_k - p_1^v(t_0)\|_2 s_l(t_0) + \|p_l - p_1^v(t_0)\|_2 s_k(t_0)}{\|p_k - p_1^v(t_0)\|_2 + \|p_l - p_1^v(t_0)\|_2} \tag{8}$$

where $s_k(t_0)$ denotes the signal value of the *j*-th measurement microphone at t_0.

MEASUREMENT SETUP

Test Samples

As this project aims to the detection of acoustical sources on a CRF, a fan with conventional blades is measured in the first step. Figure 3 shows Sample 1. The design parameters are presented in Table 1. Both the measured performance and the measured acoustics will be the reference for all further investigations.

The blade couples for impeller A and impeller B of all the design samples investigated are shown in Figure 4. The first one is a conventional blade couple (Sample 1). The design of the first sample has been carried out by using the program CFturbo [14]. The second sample uses the same blades but with serrations at the trailing edge [6, 7] at rotor A.

Table 1: design parameters of the CRF

Parameter		**Impeller A**	**Impeller B**	**CRF**
Hub Diameter [mm]	D_H	195		
Fan Diameter [mm]	D_S	307		
Number of Vanes [--]	z	7	5	
Rotation Speed [s^{-1}]	n	32	20	25.3[1]
Volume flow [$m^3\ s^{-1}$]	Q	0.486		
Total pressure rise [Pa]	Δp_t	120	60	180
Flow number	$\varphi = \frac{4Q}{\pi {D_S}^2 u}$[2]	0.21	0.27	0.27
Pressure number	$\Psi = \frac{2\Delta p_t}{\varrho u^2}$	0.21	0.27	0.50
Dimensionless Diameter	$\delta = \frac{\Psi^{0.25}}{\varphi^{0.5}}$	1.47	1.23	1.62
Dimensionless Speed	$\sigma = \frac{\varphi^{0.5}}{\Psi^{0.75}}$	1.49	1.56	0.87

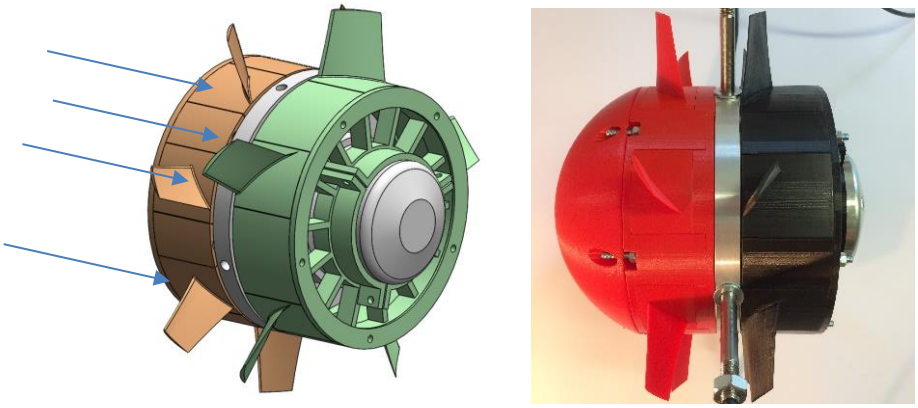

Figure 3: computer-graphics of the Sample 1 and manufactured Version (flow from left to right)

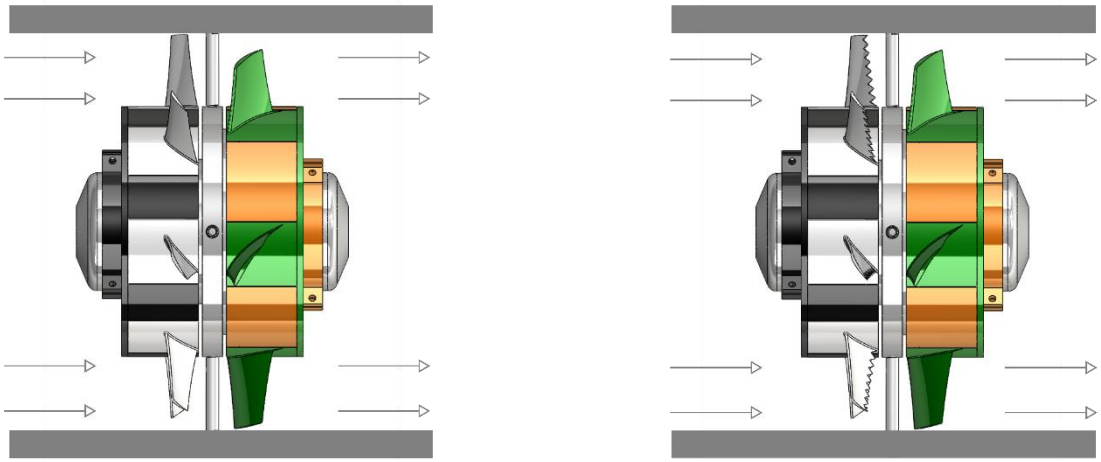

Figure 4: design studies under examination, Sample 1 with "standard" vanes for rotor A and B (left) and Sample 2 with serrations at the trailing edge at rotor A (right)

[1] $n_{CRF} = \sqrt{n_A\, n_B}$

[2] $u = \pi D_S n$

Test Stand

The measurements were carried out at a test stand generally according to ISO 5081 [5]. Category C was selected as mode of installation, implying that there is a pipe at the suction side and a free outlet at the pressure side of the fan. Deviating to the standard, a silencer was installed in front of the fan. The installation of the silencer is necessary for to the acoustic measurements, but shall have no influence on the fan operation itself. A schematic drawing of the test stand is presented in Figure 5. To meet the design point of fan operation the pressure drop is adjustable by means of a throttle valve. The flow rate was measured by means of the inlet nozzle and the static pressure rise utilizing the static pressure difference at the suction side of the fan against the environment. The rectifier was installed to achieve a constant and equal velocity profile. The silencer is employed for reducing disturbances by reflection of noise towards the suction side of the fan. The fan was hold by a 4-arm hub.

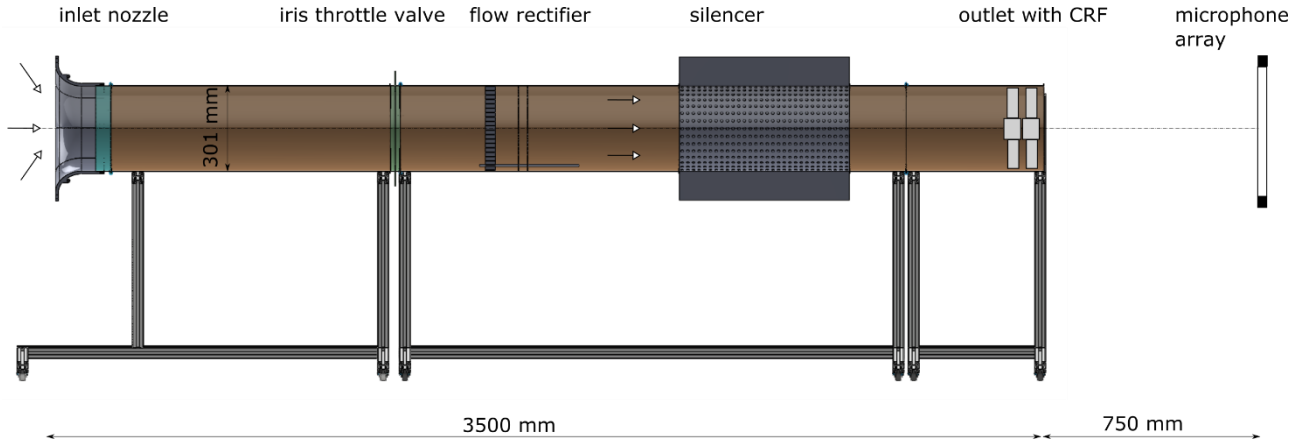

Figure 5: schematic drawing of the test stand

Figure 6 shows the measurement setup in a semi-anechoic room. An Acoustic Camera was placed at a distance of 0.75 m looking directly towards the pressure side of the fan. In order to receive precise results an accurate positioning of the array is needed. A concentric relationship between the microphone ring and the air duct as well as parallel relationship between the plane of the fan outlet and the plane of the microphones had been established by measuring and adjusting the distances between the hub center and the microphones.

As the rotational beamforming algorithm uses a virtual microphone rotation symmetric array geometries shall be preferred. A 48-channel ring-array with a diameter of 0.75 m was used here. The rotation speeds of the impellers were recorded with two laser rpm-meter facing towards the impellers from either side of the test stand.

Figure 6: microphone array in front of the pressure side of the CRF

MEASUREMENT RESULTS

Performance

The results obtained by the performance tests are presented in Figure 7. Throughout the measurement the rotational speeds have been fixed at $n_A = 32\ s^{-1}$ and $n_B = 20\ s^{-1}$.

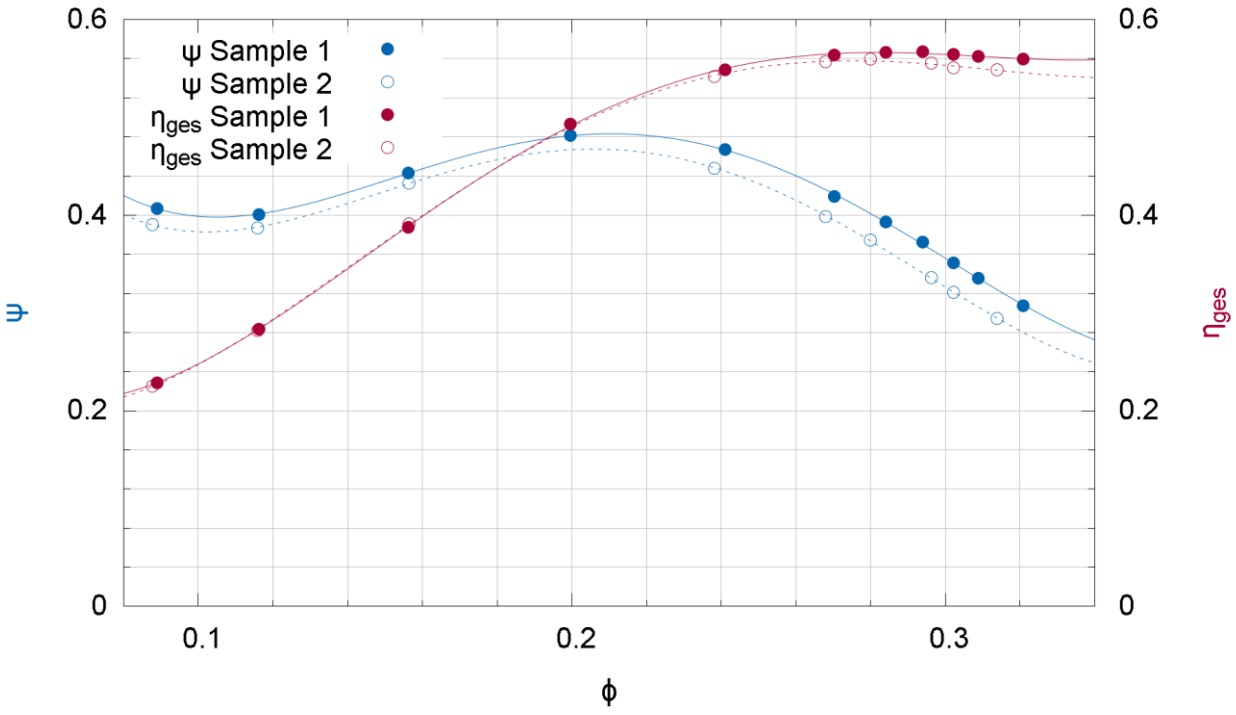

Figure 7: flow number vs. pressure number and total efficiency of Sample 1 (continuous line and filled points) and Sample 2 (dashed line and empty points).

The maximum efficiency $\eta_{ges} = \frac{Q\ \Delta p_t}{P_{el}}$ is obtained at $\varphi = 0.28$. The resulting pressure number is $\Psi = 0.4$. In comparison to the parameters presented in Table 1, design point and best point of operation are fitting sufficiently.

The subsequent measurements have been carried out using a constant volume flow at 0,486 m³/s.

Noise

The acoustic measurements are completely carried out with rotational beamforming. Orthogonal as well as functional beamforming was applied in a separate step for increasing the dynamic range in same cases.

Acoustic images of the 5 kHz and the 2 kHz third octave band are shown below. In accordance to section “Functional Beamforming” the measured signals have to be rotated virtually with the rotational speed according to the rotational direction of the specific impeller. Due to the contra rotating working principle of impeller A and impeller B two acoustic images have to be calculated at every third octave band and for each test sample.

Figure 8 depicts the acoustic images of the 5 kHz third octave band. The upper row shows the impeller A (direction of rotation: clockwise) and the lower row shows the impeller B (direction of rotation: counter-clockwise). The left column represents Sample 1 with standard vanes and the right column represents the Sample 2 with serrations at the trailing edge on impeller A.

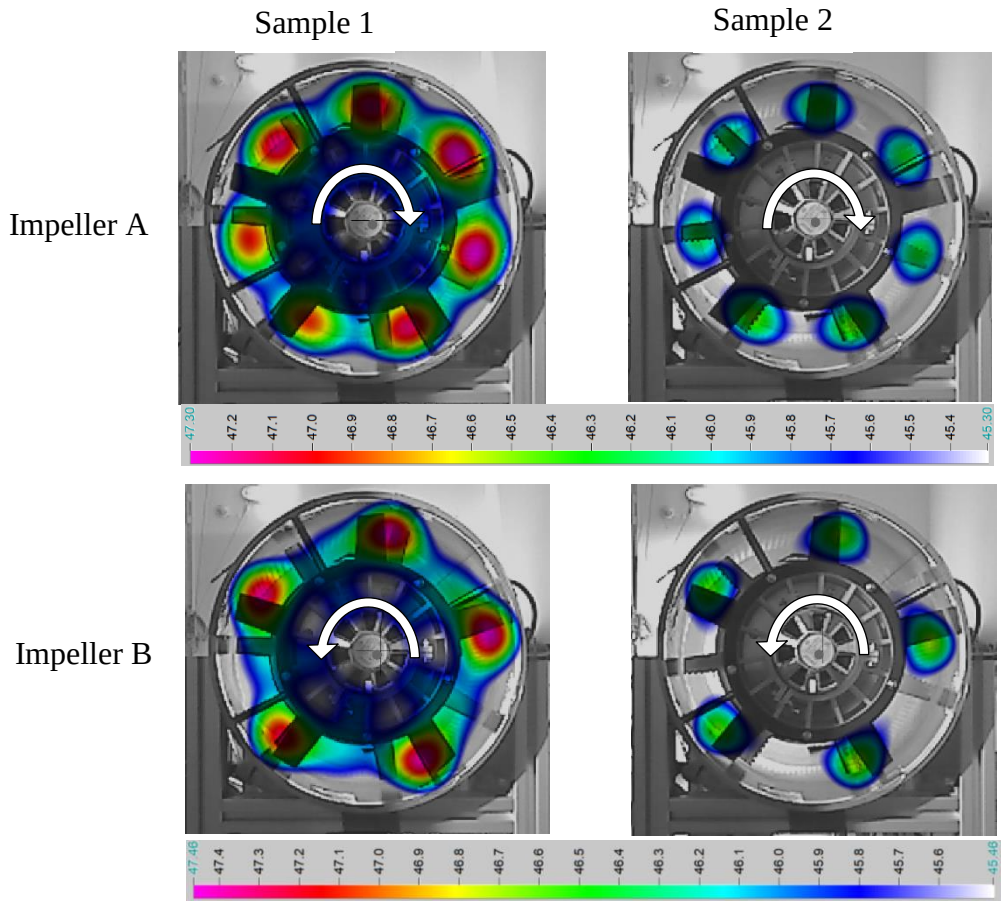

Figure 8: acoustic image of the 5 kHz third octave band, Sample 1 with standard vanes (left) and Sample 2 with vanes with serrations at the trailing edges (right), impeller A (above) and impeller B (below)

The sound sources at impeller A and impeller B are visible by applying Rotational beamforming. Corresponding to the amount of vanes at impeller A seven single aero-acoustic sources and at impeller B five single aero-acoustic sources can be localised.

The aero-acoustic sound sources at impeller A (small vanes) are always located at the trailing edge in the middle of the span in case of Sample 1. At Sample 2 the aero-acoustic sound sources are situated in the middle between leading and trailing edge. In radial direction the source location is near to the hub.

The aero-acoustic sound source of impeller B is the trailing edge, for Sample 1 as well as for Sample 2. Obviously the differences in both samples (vanes of impeller A) have no measurable influence on the sound source position at impeller B.

The measured difference in the sound pressure level between Sample 1 and Sample 2 is in the range of 1 dB.

Figure 9 shows the results for the 2 kHz third octave band.

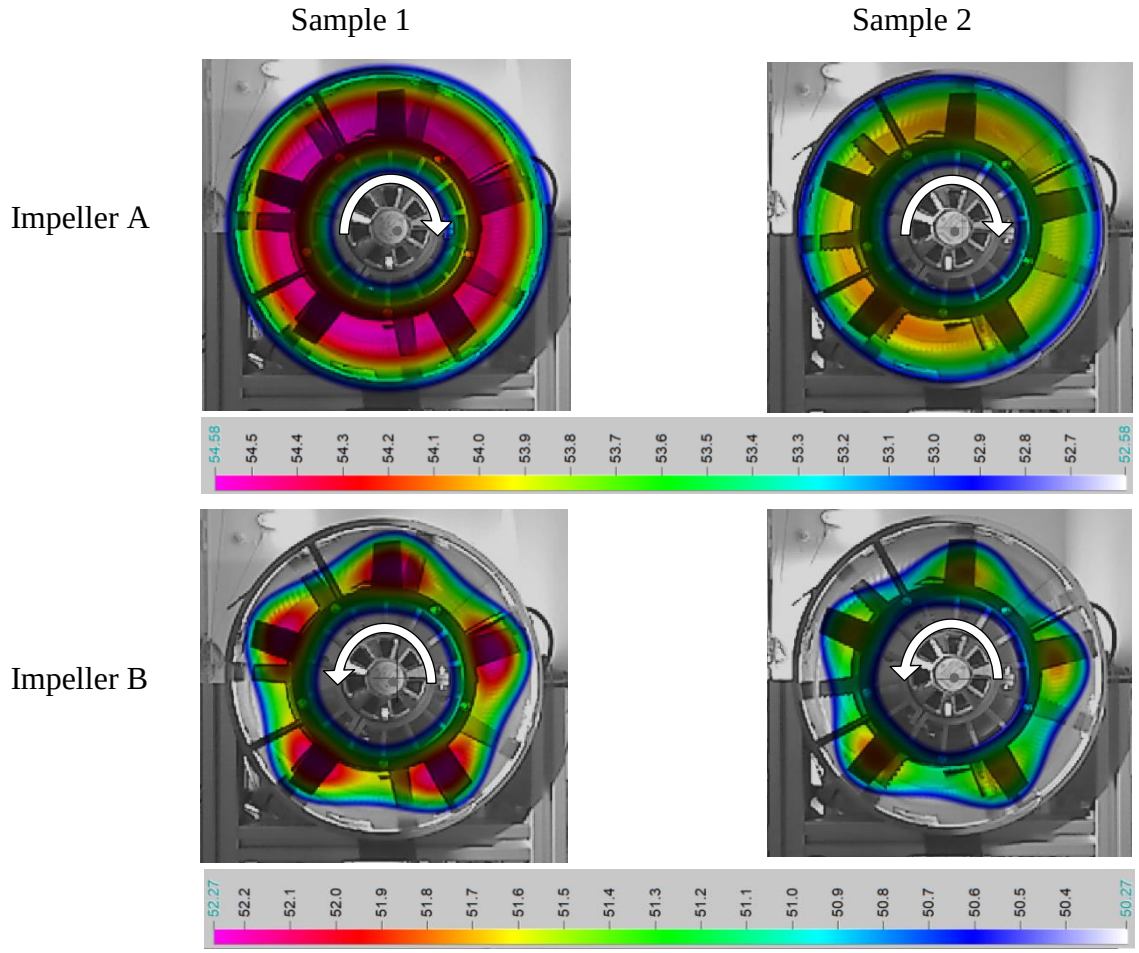

Figure 9: acoustic image of the 2 kHz third octave band, Sample 1 with standard vanes (left) and Sample 2 with vanes with serrations at the trailing edges (right), impeller A (above) and impeller B (below)

In the 2 kHz third octave band impeller B shows nearly the same acoustic behaviour as in the 5 kHz third octave band. Five noise sources can be identified clearly. In comparison to Sample 1 a reduction of the noise emission of about 1 dB is obtained using Sample 2.

Contrary to the findings at 5 kHz no specific noise sources could be detected on impeller A. The acoustic image shows a circular sound source. The noise emission of the impeller A is probably significantly lower than the noise emission of the impeller B. So the noise emission of the impeller B masks the sound sources from impeller A. In the acoustic pictures these sources from impeller B appear “smeared”, because the rotational filter was applied with the speed and direction of impeller A, while they actually belong to impeller B.

Measurement Uncertainty

The uncertainty of the performed measurements depend among other influences on the used beamforming algorithm. In [15] Sarradj evaluates the influence of different formulations of the steering vectors on the source strength and position for a three-dimensional scenario. This of course concerns the absolute source strength.

In our case the relative certainty of the measurements are of higher interest. The rotational speed of the fans are rather stable. Therefore the aero-acoustic sound induced by the impellers is relatively stable. Furthermore the measurement conditions (test stand, camera position, working point etc.) could be reproduced. Consequently one can assume that the evaluated process is highly constant, though stochastic. To avoid further deviations the integration interval for the source evaluation has been chosen quite long (32 seconds). This leads to a reliable averaging of the sound field within this time period and therefore a low measurement uncertainty when comparing different types if impellers.

To get an impression of the uncertainty level the complete measurement signal of 32 seconds length has been evaluated in 2 seconds intervals. For each interval the source strength was calculated using rotational beamforming. This was evaluated exemplarily for the acoustic image in the upper left corner of figure 8 (both impellers with standard vanes, rotating clockwise, 5 kHz third octave band). Table 2 shows the results for 16 intervals of 2 seconds length:

Table 2: Source strength of the same acoustic sound source in various two-seconds intervals

Interval	**Source Strength**	**Interval**	**Source Strength**
0-2 sec	47,52 dB	16-18 sec	47,28 dB
2-4 sec	47,41 dB	18-20 sec	47,29 dB
4-6 sec	47,39 dB	20-22 sec	47,47 dB
6-8 sec	47,30 dB	22-24 sec	47,44 dB
8-10 sec	47,19 dB	24-26 sec	47,40 dB
10-12 sec	47,22 dB	26-28 sec	47,36 dB
12-14 sec	47,28 dB	28-30 sec	47,41 dB
14-16 sec	47,34 dB	30-32 sec	47,26 dB

The source strength within the complete 32 seconds interval has been calculated with 47,30 dB (see figure 8). When averaging the 16 two-seconds intervals we get an average of 47,34 dB with a standard deviation of 0,09 dB. This difference might result from the fact that with the 32 second interval also effects of the 2 second interval limits are averaged.

Of course the uncertainty level will differ from measurement to measurement and when taking different interval lengths into account. This could be part of future investigations. The uncertainty level in the residual measurements can be assumed as similar since all boundary conditions can be reproduced with high precision.

CONCLUSION

It is possible to locate sound sources on rotating blades of a contra rotating axial fan using an Acoustic Camera in combination with a so-called rotational beamforming algorithm. Despite the contra rotating impellers sound sources can be assigned to the specific impeller. However if the noise emission of one impeller is significantly less than the contra rotating impeller the sound sources will be hidden behind a circular sound source.

It could be demonstrated, that the Sample 2 with serrations at the trailing edge leads to a reduction of the sound emission. In the third octave bands of 2 kHz and 5 kHz the reduction is about 1 dB, each.

Further investigations shall be done with sinusoidal modifications at the leading edge [8-12]. The point of interest is both the development of measurement methods to locate sound sources in contra rotating systems and understanding the mechanism of sound emission on the rotating blades of fans.

ACKNOWLEDGEMENTS

The research project is funded by the German Federal Ministry of Economic Affairs and Energy (BMWi) under the title “Primary noise reduction on a contra-rotating axial fan” (MF150166). Moreover the authors would like to thank Mr. Sven Rossol and Mr. Phil Bender for their contributions to the measurements.

Supported by:

Federal Ministry
for Economic Affairs
and Energy

on the basis of a decision
by the German Bundestag

BIBLIOGRAPHY

[1] R.P. Dougherty – *Functional beamforming* Berlin Beamforming Conference 2014, **2014**

[2] E. Sarradj – *A fast signal subspace approach for the determination of absolute levels from phased microphone array measurements* Journal of Sound and Vibration 329,1553-1569, **2010**

[3] E. Sarradj – *Three-Dimensional Acoustic Source Mapping with Different Beamforming Steering Vector Formulations* Advances in Acoustics and Vibration, **2012**

[4] P. Sijtsma – *CLEAN based on spatial source coherence* International Journal of Aeroacoustics 6, 357-374, **2007**

[5] DIN EN ISO 5801 – *Industrial fans – Performance testing using standardized airways (ISO 5801:2007, including Cor 1:2008);German version EN ISO 5801*, **2008**

[6] Carolus, Th. – *Ventilatoren – Aerodynamischer Entwurf, Schallvorhersage, Konstruktion. 3. Auflage* Springer Vieweg, ISBN 978-3-8348-2471-4, **2013**

[7] Catalano, F.M. – *Airfoil self Noise Reduction by Application of different Types of Trailing Edge Serrations* 28th International Congress of the Aeronautical Sciences, **2012**

[8] Corsini, A., Delibra, G. – *Leading Edge Bumps in Ventilation Fans* Paper No. GT2013-94853, pp. V004T10A007, doi:10.1115/GT2013-94853, **2013**

[9] Hansen, K. et al – *Reduction of Flow Induced Airfoil Tonal Noise using leading edge sinusoidal modifications* Journal of Aircraft 11:4, 197-202, doi: 10.2514/3.59219, **1974**

[10] Hersh, Alan S. et al – *Investigation of Acoustic Effects of Leading-Edge Serrations on Airfoils* Acoustics Australia 172 - Vol. 40, No. 3, **2012**

[11] Polacsek, C. et al – *Turbulence-airfoil interaction noise reduction using wavy leading edge: An experimental and numerical study* Internoise, Osaka, Japan, **2011**

[12] Soderman, P.T – *Aerodynamic effect of leading edge serrations a two-dimensional airfoil* NASA TM X-2643, **1972**

[13] Kerscher, M.; Heilmann, G.; C.Puhle; Krause, R. & Friebe, C – *Sound Source Localization on a Fast Rotating Fan Using Rotational Beamforming* INTER-NOISE, the 46th International Congress and Exposition on Noise Control Engineering, 626 (1-8), Hong Kong, China, **2017**

[14] CFturbo GmbH, – *CFturbo Version 10.3*, **2017**

[15] Sarradj, E.: *Three-Dimensional Acoustic Source Mapping with Different Beamforming Steering Vector Formulations;* Advances in Acoustics and Vibration, Volume 2012 (2012), Article ID 292695, 12 pages, **2012**